

A vibration model residual-based sequential probability ratio test framework for structural health monitoring

Fotis P Kopsaftopoulos¹ and Spilios D Fassois²

Abstract

The goal of this study is the introduction and experimental assessment of a sequential probability ratio test framework for vibration-based structural health monitoring. This framework is based on a combination of binary and multihypothesis versions of the statistically optimal sequential probability ratio test and employs the residual sequences obtained through a *single* stochastic time series model of the healthy structure. The full list of properties and capabilities of the sequential probability ratio test is for the first time presented and explored in the context of vibration-based damage diagnosis. The approach postulated in this framework is shown to achieve early and robust damage detection, identification (classification), and quantification based on predetermined sampling plans, which are both analytically and experimentally compared and assessed. The framework's performance is determined a priori via the use of the analytical expressions of the operating characteristic and average sample number functions in combination with baseline data records. It is shown to require, on average, a minimal number of signal samples in order to reach a decision compared to fixed sample size most powerful tests. The effectiveness of the proposed approach is validated and experimentally assessed via its application to a lightweight aluminum truss structure.

Keywords

Structural health monitoring, damage detection, damage identification, statistical time series methods, sequential methods, vibration-based methods

Introduction

Vibration-based damage detection, identification, and quantification, also collectively referred to as damage diagnosis, are of paramount importance for reasons associated with proper operation, reduced maintenance costs, increased safety, and improved dynamic performance.^{1–3} The process of implementing a damage diagnosis and—in certain cases—prognosis strategy is referred to as structural health monitoring (SHM). It involves the online (sometimes periodical) monitoring of a structure, the extraction of damage sensitive quantities from collected signals (measurements), and the statistical analysis of these quantities in order to determine the current health state of the structure and estimate its remaining useful service life.

The need for global damage diagnosis methods that can be applied to “real” structures has led to the development of methods that examine changes in the

structural vibration characteristics. Vibration-based SHM methods are among the most accurate and effective.^{2–7} Statistical time series SHM methods form an important and rapidly evolving class, within the broader vibration-based family of methods. Their three *main elements* are as follows: (1) random excitation and/or vibration response signals (*time series*), (2) statistical model building, and (3) statistical decision

¹Structures and Composites Laboratory (SACL), Department of Aeronautics & Astronautics, Stanford University, Stanford, CA, USA

²Stochastic Mechanical Systems & Automation (SMSA) Laboratory, Department of Mechanical & Aeronautical Engineering, University of Patras, Patras, Greece

Corresponding author:

Spilios D Fassois, Stochastic Mechanical Systems & Automation (SMSA) Laboratory, Department of Mechanical & Aeronautical Engineering, University of Patras, Patras, GR 265 04, Greece.
 Email: fassois@mech.upatras.gr

making for inferring the health state of a structure. They offer a number of potential advantages, including no requirement for physics-based or finite element (FE) models as they are *data-based* (inverse type) methods, no requirement for complete modal models, effective treatment of uncertainties, and statistical decision making with specified performance characteristics.^{5,6,8–10}

Statistical time series methods for SHM are based on random (stochastic) vibration signals under healthy and potentially damage structural states, identification of suitable time series models describing the dynamics in each state, and extraction of a statistical characteristic quantity characterizing the structural state in each case (baseline phase). Damage diagnosis is accomplished in the inspection phase via statistical decision making consisting of comparing, in a statistical sense, the current characteristic quantity with that of each potential state as determined in the baseline phase. Non-parametric time series methods are those based on the corresponding non-parametric time series representations, such as spectral estimates (power spectral density (PSD), frequency response function (FRF)).^{9,11–14} On the other hand, parametric time series methods are those based on the corresponding parametric time series representations, such as the autoregressive moving average (ARMA) models^{15,16}, and their principles have been used in a number of studies.^{8,9,17–22} For an extended overview of the main statistical time series methods for SHM, the interested reader is referred to Fassois and Sakellariou,^{5,6} while experimental assessments of various scalar and vector methods are provided in Kopsaftopoulos and Fassois.^{9,23}

The vast majority of statistical time series SHM methods is based on fixed sample size (FSS) hypothesis testing procedures which are used in the statistical decision making. FSS hypothesis testing employs a constant amount of observations, which is determined a priori of the experimental data acquisition. On the other hand, sequential methods have the feature that the number of observations required by the procedure is not determined in advance of the experiment. The decision to terminate the experiment depends, at each stage, on the results of the observations previously made, thus the number of observations required by the test is not predetermined, but a *random variable*. If samples can be taken one at a time and the information from them accumulated, one would expect to be in a better position to make decisions than if no attempts were made to look at the data until a sample of fixed size had been taken. A merit of the sequential method, as applied to testing statistical hypotheses, is that test procedures can be constructed which require, on average, a substantially smaller number of observations than equally reliable test procedures based on a predetermined (fixed) number of observations.^{24–26} Moreover, a potential

advantage of a damage diagnosis method based on sequential procedures is its straightforward extension for online implementation, which may be of great interest with respect to the current SHM application requirements.

In 1947, Wald²⁴ introduced the sequential probability ratio test (SPRT), which is a statistically optimal test in the sense that it minimizes the expected sample size (stopping time of the test) both under the null and under the alternative hypotheses among all tests with the same or smaller error probabilities and with finite expected sample sizes under the two hypotheses.^{25–27} Although the SPRT was introduced over half a century ago, its engineering applications have been limited to the surveillance of nuclear power plant components,^{28,29} while some numerical investigations of its performance with respect to anomaly detection in nuclear reactor noise signals have been presented in Schoonewelle et al.^{30,31} and Glöckler.³² In the context of vibration-based damage diagnosis and SHM, preliminary—with respect to the use of an SPRT scheme—studies include Sohn et al. and Oh and Sohn,^{18,33} where the binary form of the SPRT based on autoregressive (AR)–autoregressive with exogenous excitation (ARX) model residuals has been applied for damage detection in a laboratory three-story building model and an 8-degree-of-freedom mass–spring system, respectively.

Although often more than two hypotheses are considered (for instance, corresponding to three different types of structural damage), thus defining a multihypothesis testing problem, most current SHM methods treat it via pairwise binary hypothesis tests.⁹ This is, obviously, an approximate procedure leading to statistically suboptimal solutions and ineffective use of the available data records. Proper sequential multihypothesis testing is treated only in a very limited number of studies in some other technical areas (such as target detection in multiple resolution radar³⁴ and infrared systems,³⁵ and signal acquisition in direct sequence code-division multiple access systems³⁶).

The goal of this study is the introduction and experimental assessment of an SPRT time series–based SHM framework capable of achieving effective, early, and robust damage detection, identification (classification), and quantification under uncertainties. In the context of this work, “early” damage detection refers to the ability of the approach to detect damage shortly after its occurrence—in the current sequential framework, this is quantified as the number of (sequentially processed) data samples needed before a decision is made. “Robust” is used to imply the approach ability to operate under (the practically inevitable) uncertainties, as well as its ability to operate properly with sensors that are either “local” (in the vicinity of) or “remote” (not

in the vicinity of) to damage. The term “effective” mainly refers to the achieved performance of the approach in terms of correct damage detections and classifications. The postulated framework employs a combination of binary and multihypothesis versions of the statistically optimal SPRT. Its basis consists of the residual sequences obtained through a *single* stochastic time series model of the healthy structural dynamics. Moreover, a complete account of properties and capabilities of the SPRT are—for the first time—presented and explored in the context of vibration-based SHM. The performance of the developed approach is determined a priori via the analytical expressions for the operating characteristic (OC) and average sample number (ASN) functions in combination with baseline data records obtained under healthy and various damage structural states.

The effectiveness of the proposed framework is experimentally assessed via its application to damage diagnosis on a lightweight aluminum truss structure. The results are presented for *three* distinct vibration response measurement positions, with a single measurement used at a time, and confirm its ability to operate based even on a single pair of measured excitation–response signals. The damage cases considered correspond to the loosening of various bolts connecting certain of the truss elements. Random force excitation is provided via an electromechanical shaker, while the vibration responses are measured at various positions via dynamic strain gauges. The main features and operational characteristics of the postulated framework are discussed along with practical issues, while its effectiveness is demonstrated via various test cases corresponding to different experiments, damage types, and vibration measurement positions.

The main issues addressed in this article are summarized as follows:

- (a) Use—for the first time in the vibration-based SHM context—of a combination of the binary and multihypothesis SPRT in order to propose a complete SHM framework able to achieve effective, early, and robust damage detection, identification, and quantification under uncertainties using a *single* stochastic time series model.
- (b) The framework’s performance is determined a priori via the use of the OC and ASN functions, selected type I (false alarm) and II (missed damage) error probabilities, and available baseline data records under various structural states.
- (c) Assessment of the framework in terms of its damage detection and identification capability under experimental uncertainties and various damage scenarios; *multiple* vibration measurement locations, which are either “local” or “remote” with

respect to damage location, are employed; large number of experiments under each scenario (1200 data records for the healthy structure and 900 data records for each considered damage out of a total of five types).

The rest of this article is organized as follows: the SPRT framework for SHM is presented in section “An SPRT framework for SHM,” while the experimental setup is presented in section “The experimental setup.” The experimental application and assessment is presented in section “Damage detection, identification and quantification results,” while the concluding remarks are finally summarized in section “Concluding remarks.”

An SPRT framework for SHM

Like all statistical time series SHM methods,^{5,6} the SPRT time series framework consists of two phases: (a) an initial *baseline phase*, which includes modeling of the healthy structure (modeling of the structure under predetermined damage types may sometimes be necessary; see section “Damage identification and quantification” for details) via a *single* stochastic time series model, and (b) the *inspection phase*, which is performed during the structure’s service cycle or continuously (online), and includes the functions of damage detection, identification, and quantification.

The workframe

Let S_o designate the structure under consideration in its *nominal* (healthy) state, S_A, S_B, \dots , the structure under damage of *type A, B*, and so on, and S_u the structure in an unknown (to be determined) state. Each damage type may, generally, include a continuum of damages characterized by common nature or location, for instance, damage of various magnitudes in a specific structural element. Yet this is considered in this study, thus the broader damage identification problem is presently treated as a (simpler) classification problem.

The postulated SPRT framework is based on discretized, scalar or vector, excitation $x[t]$, and/or response $y[t]$ (for $t = 1, 2, \dots$) random vibration data records (note that t refers to discrete time, with the corresponding actual time being $(t - 1)T_s$, where T_s stands for the sampling period). Like before, a subscript (o, A, B, \dots, u) is used for designating the corresponding structural state that provided the signals. Note that all collected signals need to be suitably pre-processed.^{5,6,16} This may include low or bandpass filtering within the frequency range of interest, signal subsampling (in case the originally used sampling frequency is too high), sample mean subtraction, as well as proper scaling (in the linear dynamics case). The latter is not only used for

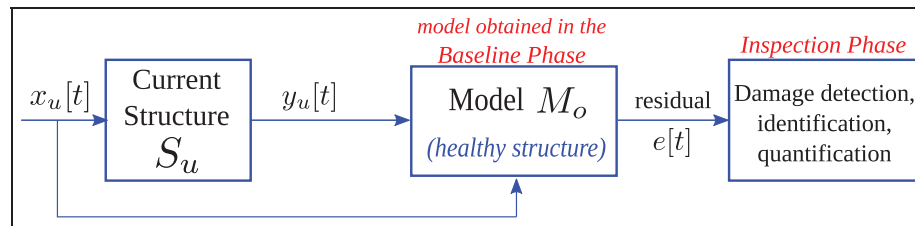


Figure 1. Schematic representation of the SPRT framework.

numerical reasons but also for counteracting—to the extent possible—different operating (including excitation levels) and/or environmental conditions.

Damage detection, identification, and quantification are based on the residual sequence obtained by driving the current (unknown) signal(s) $x_u[t]$, $y_u[t]$ through a *single*, predetermined in the baseline phase, model M_o corresponding to the healthy structural state. Let the residual sequence obtained by driving the current signals $x_u[t]$, $y_u[t]$ through the healthy model M_o be designated as $e[t]$ and characterized by variance σ^2 . The general idea is that the residual sequence obtained by a model that truly reflects the actual (current) structural state will be characterized by a minimal standard deviation.

Figure 1 presents a schematic representation of the SPRT framework.

Baseline phase

Baseline modeling of the structural dynamics. Data records from the healthy structure are employed for the identification and validation of appropriate parametric time series models, which may be scalar (univariate) models in the case of a single vibration response measurement position or vector (multivariate) models (or suboptimally an array of scalar models) in the case of several vibration response measurement positions. In the *response-only* case, AR or ARMA models may be employed,³⁷ which may be alternatively set into state-space form.^{15,37} In the excitation–response case, ARX or autoregressive moving average with exogenous excitation (ARMAX) models may be used^{15,16} or their corresponding state-space representations.¹⁵

In this study, a single measurement position, and a corresponding scalar (single excitation and single response) ARX model, is used at a time. An ARX(na , nb) model is of the form (lower case/capital bold face symbols designate vector/matrix quantities, respectively)^{15,16}

$$y[t] + \sum_{i=1}^{na} a_i \cdot y[t-i] = \sum_{i=0}^{nb} b_i \cdot x[t-i] + e[t] \quad (1)$$

$$e[t] \sim \text{iid } \mathcal{N}(0, \sigma^2)$$

with t designating the discrete time; $x[t]$ and $y[t]$ are the measured excitation and vibration response signals, respectively; na and nb are the AR and exogenous (X) orders, respectively; and $e[t]$ is the stochastic model residual (one-step-ahead prediction error (PE)) sequence, that is a white (serially uncorrelated), Gaussian, zero mean with variance σ^2 sequence, uncorrelated with the excitation $x[t]$. The symbol $\mathcal{N}(\cdot, \cdot)$ designates Gaussian distribution with the indicated mean and variance, and iid stands for identically independently distributed.

The model is parameterized in terms of the parameter vector $\theta = [a_i; b_i; \sigma^2]^T$ to be estimated from the measured signals.^{15,16} Model estimation may be achieved based on minimization of the ordinary least squares (OLS) or the weighted least squares (WLS) criteria.^{15,16} The modeling procedure involves the successive fitting of ARX(na , nb) models for increasing orders na and nb , until an adequate model is selected.¹⁶ Model order selection, which is crucial for successful identification, may be based on the Bayesian information criterion (BIC), which is a statistical criterion that penalizes model complexity (order) as a counteraction to a decreasing quality criterion^{15,16}

$$\text{BIC} = \ln \hat{\sigma}^2 + (na + nb) \times \frac{\ln L}{L} \quad (2)$$

where $\hat{\sigma}^2$ stands for the estimate of the residual signal variance and L the signal length (in samples). Other useful tools in this context include monitoring the residual sum of squares/signal sum of squares (RSS/SSS), the residual autocorrelation function,¹⁵ and also “stabilization diagrams” which depict the estimated modal parameters (usually frequencies) as a function of increasing model order.¹⁶ Final model validation is based on formal verification of the residual sequence uncorrelatedness (whiteness) hypothesis.¹⁵

Inspection phase

Let $x_u[t]$, $y_u[t]$ ($t = 1, 2, \dots$) represent the current excitation and response signals, respectively, obtained from the structure in an *unknown* (to be classified) state. Damage detection, identification, and quantification are based on the single, predetermined in the baseline

phase, time series model of the healthy structure (M_o). The current excitation and response signals are driven through this model and estimates of the current residual series $e[t]$ are obtained. Subsequently, these estimates are used for tackling the damage detection, identification, and quantification tasks.

Damage detection. Damage detection is based on the binary SPRT introduced in Wald,²⁴ which is used in order to detect a change in the standard deviation σ of the model residual sequence obtained by driving the current (unknown) excitation and response signals through the baseline healthy model M_o . By using the SPRT, it is possible to specify two values σ_o and σ_1 for the residual standard deviation, such as the classification of the structure as healthy is considered whenever $\sigma \leq \sigma_o$, while the classification of the structure as damaged is considered whenever $\sigma \geq \sigma_1$. The zone between σ_o and σ_1 constitutes an *uncertainty zone*, thus for σ lying within this zone the decision is postponed and data collection continues.

The probability of classifying the structure as damaged when it is actually healthy should not exceed a preassigned value α whenever $\sigma \leq \sigma_o$ (*false alarm* or *type I error probability*), while the probability of classifying the structure as healthy when it is actually damaged should not exceed a preassigned value β whenever $\sigma \geq \sigma_1$ (*missed damage* or *type II error probability*). The values of σ_o and σ_1 are user defined and express the increase of the standard deviation ratio $q = \sigma_1/\sigma_o$ for which the structure is considered to be in a damage state. For example, a ratio of $q = 1.1$ means that the structure is considered damaged whenever there is an increase of 10% in the standard deviation σ of the current residual sequence compared to a threshold value σ_o .

Damage detection is based on the following hypothesis testing problem implemented via the SPRT of strength (α, β) , with α, β designating the type I (false alarm) and II (missed damage) error probabilities, respectively:

$$\begin{aligned} H_o &: \sigma \leq \sigma_o \text{ (null hypothesis – healthy structure)} \\ H_1 &: \sigma \geq \sigma_1 \text{ (alternative hypothesis – damaged structure)} \end{aligned} \tag{3}$$

with σ_o, σ_1 designating the user-defined values.

Under the null hypothesis, the residuals $e[t]$ are iid zero mean Gaussian with variance σ^2 , hence

$$\text{Under } H_o : e[t] \sim \text{iid } \mathcal{N}(0, \sigma^2), \quad t = 1, 2, \dots \tag{4}$$

and the probability density function of the residual sequence $e[t]$ is given by

$$f(e[t]|\sigma) = \frac{1}{(2\pi)^{\frac{t}{2}}\sigma^t} \exp\left\{-\frac{1}{2\sigma^2} \sum_{l=1}^t e^2[t]\right\}. \tag{5}$$

The likelihood ratio is computed at each stage t of the experiment as follows

$$\begin{aligned} \frac{\mathcal{L}(\sigma_1|e[1], \dots, e[t])}{\mathcal{L}(\sigma_o|e[1], \dots, e[t])} &= \frac{\prod_{l=1}^t f(e[l]|\sigma_1)}{\prod_{l=1}^t f(e[l]|\sigma_o)} = \frac{\frac{1}{(2\pi)^{\frac{t}{2}}\sigma_1^t} \exp\left\{-\frac{1}{2\sigma_1^2} \sum_{l=1}^t e^2[t]\right\}}{\frac{1}{(2\pi)^{\frac{t}{2}}\sigma_o^t} \exp\left\{-\frac{1}{2\sigma_o^2} \sum_{l=1}^t e^2[t]\right\}}. \end{aligned}$$

Taking logarithms and dividing by $(1/2\sigma_o^2) - (1/2\sigma_1^2)$, the logarithm of the likelihood ratio is obtained

$$\Lambda[t] = t \cdot \log \frac{\sigma_o}{\sigma_1} + \frac{\sigma_1^2 - \sigma_o^2}{2\sigma_o^2\sigma_1^2} \cdot \sum_{l=1}^t e^2[t]. \tag{6}$$

The basis of the SPRT is the logarithm of the likelihood ratio function with $\Lambda[t]$ designating the decision parameter—or equivalently, the test statistic—of the method at sample t . Hence, the following test of strength (α, β) may be constructed

$$\begin{aligned} \Lambda[t] \leq \log B & \quad \text{accept } H_o \text{ (healthy structure)} \\ \Lambda[t] \geq \log A & \quad \text{accept } H_1 \text{ (damaged structure)} \\ \log B < \Lambda[t] \leq \log A & \quad \text{no decision is made (continue the test)} \end{aligned} \tag{7}$$

with $A = (1 - \beta)/\alpha$ and $B = \beta/(1 - \alpha)$,²⁴ and $\log A, \log B$ designating the upper and lower, respectively, critical points (thresholds) of the test.

Following a decision at a stopping time \hat{N} , it is possible to continue the test by resetting $\Lambda[\hat{N} + 1]$ to 0 and continue the experiment by using additional residual samples. Thus, by using finite vibration response data records $x_{ul}[t], y_{ul}[t]$ with $t = 1, 2, \dots, K$ and the corresponding residual sequences, the SPRT is capable of making additional decisions (if this is deemed necessary), as the test statistic Λ resets to 0 after a damage is detected.

The OC function. For any value of the residual standard deviation σ , the OC function $L(\sigma)$ denotes the probability that the SPRT for damage detection will terminate with the acceptance of the null hypothesis H_o that the structure is in a healthy state. The OC function is defined as^{24,38}

$$L(\sigma) = \frac{\left(\frac{1-\beta}{\alpha}\right)^h - 1}{\left(\frac{1-\beta}{\alpha}\right)^h - \left(\frac{\beta}{1-\alpha}\right)^h} \tag{8}$$

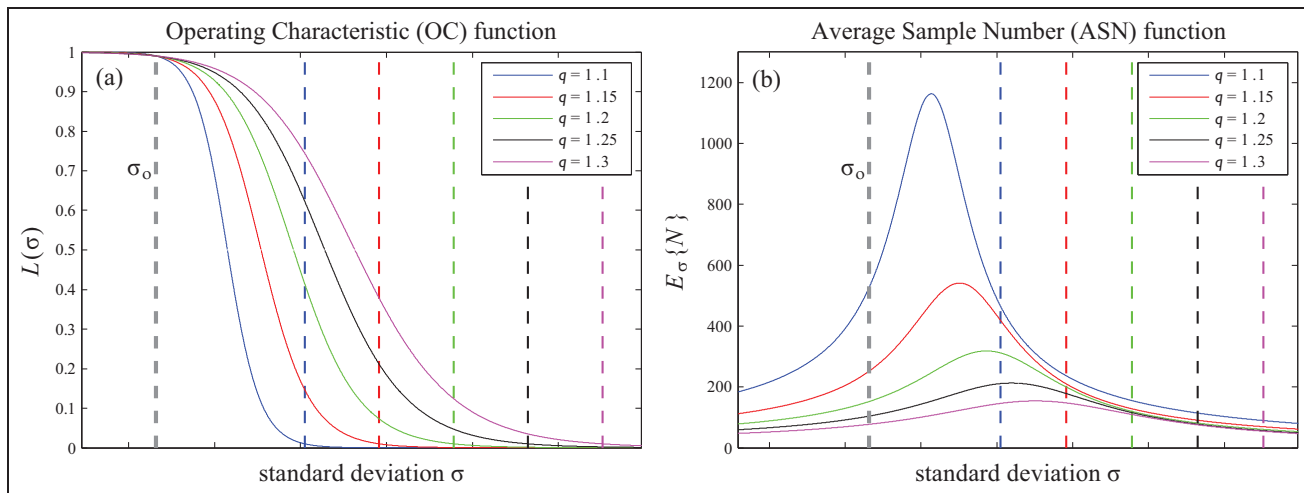


Figure 2. (a) Operating characteristic (OC) and (b) average sample number (ASN) functions for various residual standard deviation ratios $q = \sigma_1/\sigma_o$ and constant strength $(\alpha, \beta) = 0.01$. The vertical colored dashed lines designate the σ_1 values for the corresponding ratios q .

where h is the root of the equation

$$\frac{1}{\sqrt{2\pi}\sigma} \frac{\sigma_o^h}{\sigma_1^h} \int_{-\infty}^{+\infty} \left(\frac{\exp\left\{-\frac{1}{2\sigma_1^2} e^2[t]\right\}}{\exp\left\{-\frac{1}{2\sigma_o^2} e^2[t]\right\}} \right)^h \exp\left\{-\frac{1}{2\sigma^2} e^2[t]\right\} de = 1 \tag{9}$$

and

$$\sigma = \sqrt{\frac{\left(\frac{\sigma_o}{\sigma_1}\right)^{2h} - 1}{\frac{h}{\sigma_1^2} - \frac{h}{\sigma_o^2}}} \tag{10}$$

Using equations (8) and (10), the OC function curve may be plotted by computing the pair $(\sigma, L(\sigma))$ for a sequence of values h , which has to be sufficiently large in order to obtain enough OC function points.

Figure 2(a) presents the OC function for various residual standard deviation ratios $q = \sigma_1/\sigma_o$ and constant strength (α, β) , while Figure 3(a) presents the OC function for various strengths (α, β) and constant residual standard deviation ratio $q = \sigma_1/\sigma_o = 1.1$. By calculating the OC function for various candidate SPRT sampling plans using various residual standard deviation ratios $q = \sigma_1/\sigma_o$ (see Figure 2(a)) and strengths (α, β) (see Figure 3(a)), the user is able to determine the corresponding probabilities of acceptance of the null hypothesis H_o (healthy structure) and thus compare in a systematic way the various sampling plans. Moreover, in the case that a number of baseline healthy data records is available, the user may estimate the corresponding residual standard deviations and check the

probability that the candidate SPRT sampling plans will determine that they indeed belong to the healthy structural state. This way, using the available baseline data records, the behavior of various SPRT sampling plans may be investigated with respect to damage detection robustness and potential false alarm rates, and the sampling plan with the best performance may be selected for final implementation.

The ASN function. The ASN function represents the average number of inspection samples required by the SPRT to reach a decision. As the number of observations required by a sequential test is not predetermined, but a *random variable*, the ASN is an approximation of the expected value $E_{\sigma}\{N\}$ of the number of residual samples required by a sampling plan of strength (α, β) and residual standard deviations σ_o, σ_1 in order to reach a terminal decision.

The expected value of the ASN function may be obtained as²⁴

$$E_{\sigma}\{N\} \approx \frac{L(\sigma) \log \frac{\beta}{1-\alpha} + [1 - L(\sigma)] \log \frac{1-\beta}{\alpha}}{E_{\sigma}\{z\}} \tag{11}$$

where

$$z = \frac{\frac{1}{\sigma_1} \exp\left\{-\frac{1}{2\sigma_1^2} e^2[t]\right\}}{\frac{1}{\sigma_o} \exp\left\{-\frac{1}{2\sigma_o^2} e^2[t]\right\}} = \log \frac{\sigma_o}{\sigma_1} + \frac{1}{2} \left(\frac{1}{\sigma_o^2} - \frac{1}{\sigma_1^2} \right) e^2[t]. \tag{12}$$

$E_{\sigma}\{z\}$ denotes the expected value of the likelihood ratio when σ is the standard deviation of the residual sequence, hence

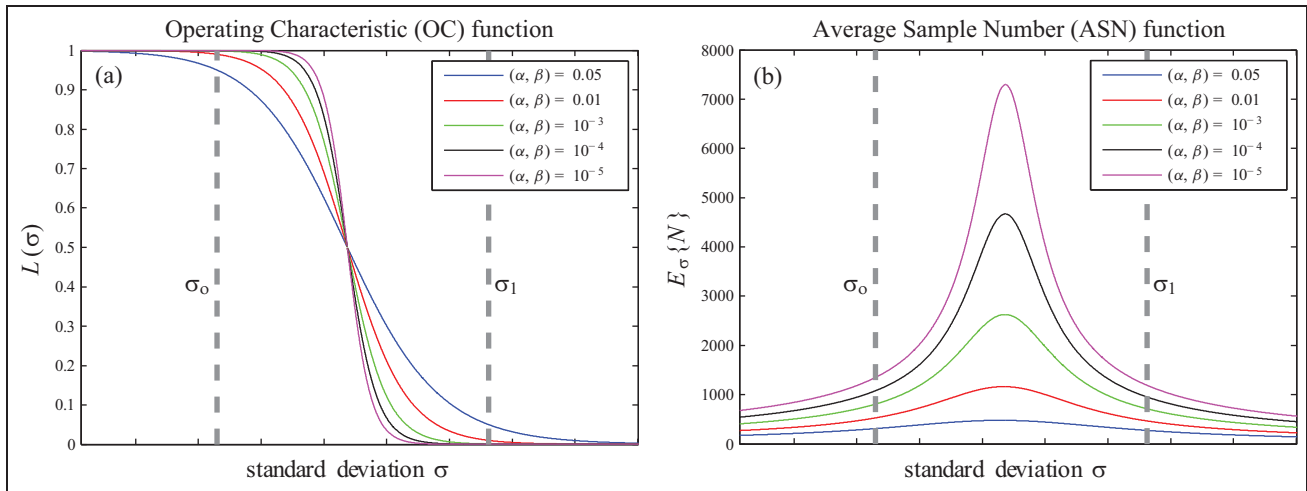


Figure 3. (a) Operating characteristic (OC) and (b) average sample number (ASN) functions for various strengths (α, β) and constant residual standard deviation ratio $q = \sigma_1/\sigma_o = 1.1$.

$$\begin{aligned}
 E_{\sigma}\{z\} &= \log \frac{\sigma_o}{\sigma_1} + \frac{1}{2} \left(\frac{1}{\sigma_o^2} - \frac{1}{\sigma_1^2} \right) E\{e^2[t]\} \\
 &= \log \frac{\sigma_o}{\sigma_1} + \frac{1}{2} \left(\frac{1}{\sigma_o^2} - \frac{1}{\sigma_1^2} \right) \sigma^2.
 \end{aligned}
 \tag{13}$$

From equations (8), (10), (11), and (13), the ASN function for various candidate SPRT sampling plans may be calculated. This is of great importance in the design of an SPRT sampling plan for damage detection, as by pre-specifying the test strength (α, β) and the residual standard deviation ratio $q = \sigma_1/\sigma_o$ for which the structure is considered to be in a damage state one may have an approximation of the expected number of residual samples that the SPRT needs in order to accept hypothesis H_o or H_1 and terminate. Hence, along with the OC function, the ASN function constitutes an additional analytical tool that may contribute to the optimal selection of an SPRT sampling plan. Figure 2(b) shows the ASN function for various residual standard deviation ratios $q = \sigma_1/\sigma_o$ and constant strength (α, β) , while Figure 3(b) depicts the ASN function for various strengths (α, β) and constant residual standard deviation ratio $q = \sigma_1/\sigma_o = 1.1$.

The SPRT of strength (α, β) minimizes, under H_o (healthy structure) and H_1 (damaged structure), the expected value $E_{\sigma}\{N\}$ of the ASN among all tests, FSS or sequential, for which the type I error (false alarm) probability is equal or less than α and the type II error (missed damage) probability is equal or less than β ^{27,38}. Thus, in order to tackle damage detection and infer the health state of a structure, based on the adopted sampling plan of the SPRT, the above procedure requires a minimum number of observations for reaching a terminal decision.

The truncated SPRT. In the case that the expected number of samples $E_{\sigma}\{N\}$, as approximated by the ASN function, indicates that an increased number of residual samples is required by the adopted SPRT sampling plan with respect to the available or “desired” number of residual samples to be employed, then a truncated version of the SPRT may be employed. The truncated SPRT may also be employed in the case where the SPRT stopping time N reaches a limit stopping time K (length of the current residual sequence $e[t]$) and still needs to continue sampling to reach a terminal decision.

The following truncated SPRT of strength (α, β) is constructed based on a user-defined stopping time K

$$\begin{aligned}
 \Lambda[K] &\leq \log \frac{1}{2} (A + B) && \text{accept } H_o \text{ (healthy structure)} \\
 \Lambda[K] &\geq \log \frac{1}{2} (A + B) && \text{accept } H_1 \text{ (damaged structure)}
 \end{aligned}
 \tag{14}$$

with $B = \beta/(1 - \alpha)$ and $A = (1 - \beta)/\alpha$.

The truncation of the SPRT will affect the type I and II error probabilities α and β , respectively, and as a result of this the strength (α, β) of the test. Nevertheless, the size of the impact on the error probabilities depends on the number of samples K based on which the SPRT is truncated.³⁸ Hence, if the truncation is implemented for a large value of K , the strength of the test will be practically unaffected. For small probabilities of type I (false alarm) and II (missed damage) errors, truncating the SPRT at stopping time K leaves the SPRT essentially unaffected when the samples are distributed under H_o (healthy structure) or H_1

the nominal healthy behavior, thus the nominal model of the healthy structure will not be able to accurately represent them, leading to increased residuals and corresponding standard deviation values. Moreover, by considering a nominal standard deviation σ_o for the healthy structure, damage detection may also be simultaneously considered. Nevertheless, in this case, the advantages of the SPRT-based damage detection approach (predetermined strength (α , β), analytical comparison of candidate sampling plans via the OC and ASN functions) will be neglected.

The experimental setup

The structure

The truss structure is suspended through a set of cords and consists of 28 elements with rectangular cross sections ($15 \times 15 \text{ mm}^2$) jointed together via steel elbow plates and bolts (Figure 4). All parts are constructed from standard aluminum with the overall dimensions being $1400 \times 700 \times 800 \text{ mm}^3$.

The force excitation is a random Gaussian signal applied vertically at Point X (Figure 4) via an electro-mechanical shaker (MB Dynamics Modal 50A, maximum load 225 N) equipped with a stinger and measured via an impedance head (PCB 288D01, sensitivity 98.41 mV/lb). The vibration responses are measured at different points via dynamic strain gauges (PCB ICP 740B02, 0.005–100 kHz, 50 mV/ $\mu\epsilon$; sampling frequency $f_s = 256 \text{ Hz}$, signal bandwidth 0.5–100 Hz). The force and strain signals are driven through a signal conditioning device (PCB 481A02) into the data acquisition system (SigLab 20–42). In this study, the damage detection, identification, and quantification results are obtained based on each one of the three vibration response signals (Points Y1, Y2, and Y3—Figure 4). This allows the examination and assessment of the proposed framework's ability to achieve damage detection, identification, and quantification with respect to the vibration response measurement positions employed. For this reason, damage is characterized as “local” or “remote” with respect to the sensor used.

The damage types and the experiments

The damages considered correspond to the complete loosening of various bolts at different joints of the structure. Five distinct types are specifically considered (Figure 4): The first damage type, referred to as *damage type A*, corresponds to the loosening of bolt A1 joining together a horizontal element with a vertical element. The second damage type, referred to as *damage type B*,

corresponds to the loosening of bolts A1 and B1 joining together an horizontal with a vertical element. Damage type B affects the same elements as damage type A, but is more severe, as loosening of two bolts is involved. The third damage type, referred to as *damage type C*, corresponds to the loosening of bolts C1 and C2 joining together an horizontal with a diagonal element. The fourth damage type, referred to as *damage type D*, corresponds to the loosening of bolt D1 joining together an horizontal with a vertical element. Finally, the fifth damage type, referred to as *damage type E*, corresponds to the loosening of bolt E1 joining together a vertical with a diagonal element. The considered damage types are summarized in Table 1.

A significant number of test cases are considered in the experimental assessment. In each test case, a specific experiment (out of a total of 1200 experiments for the healthy structure and 900 experiments for each damage state, with 100 from each category used in the baseline phase—Table 1) and a specific vibration response measurement position (Points Y1–Y3, Figure 4) are employed. Hence, the numbers of test cases correspond to the number of experiments mentioned in Table 1 times the number of measured response positions. Experimental details are presented in Table 1—worth noting is the very low/limited bandwidth used, which does not favor SHM but is presently used to comply to those situations where higher/wider bandwidths cannot be employed (for instance, when only natural or other low/limited bandwidth excitation is available). Notice that the sample mean is subtracted from each signal and scaling by the signal's sample standard deviation is implemented.

Damage detection, identification, and quantification results

Damage detection, identification, and quantification results are based on a single excitation–response signal pair for each test case. The excitation force is always measured at Point X, but the vibration response measured at one of Points Y1, Y2, or Y3 (Figure 4) is used in each test case, thus the number of test cases is three times the number of mentioned experiments. Depending on the distance of the employed sensor from the damage occurrence location, the damage is characterized either as *local* or *remote*. Of course, the interesting point being presently investigated is whether the proximity of a sensor to the damage location seems to provide a significant advantage in the damage detection robustness and the identification accuracy. The considered damage types, experiments, and other details are summarized in Table 1.



Figure 4. The aluminum truss structure and the experimental setup: the force excitation (Point X), the vibration measurement positions (Points Y1–Y3), and the considered damage types (A, B, C, D, and E).

Table 1. The considered damage types, numbers of experiments, and vibration signal details.

Structural state	Description	Total number of experiments
Healthy	–	1200 (100 baseline)
Damage type A	Loosening of bolt A1	900 (100 baseline)
Damage type B	Loosening of bolts A1 and B1	900 (100 baseline)
Damage type C	Loosening of bolts C1 and C2	900 (100 baseline)
Damage type D	Loosening of bolt D1	900 (100 baseline)
Damage type E	Loosening of bolt E1	900 (100 baseline)
Sampling frequency: $f_s = 256$ Hz, signal bandwidth: [0.5–100] Hz		
Signal length in samples (s): non-parametric analysis: 30,720 (120 s); parametric analysis: 1000 (3.9 s)		

Baseline phase: structural identification under the healthy structural state

Non-parametric identification. Non-parametric structural identification is based on 30,720 (≈ 120 s) sample-long excitation–response signals. A 2048 sample-long

Hamming data window with zero overlap is used (15 segments) for the FRF Welch-based estimation (MATLAB function *tfestimate.m*). Indicative FRF magnitude estimates for the healthy and damage structural states (Point X–Point Y1 and Point X–Point Y3 transfer functions) are depicted in Figure 5. As it may

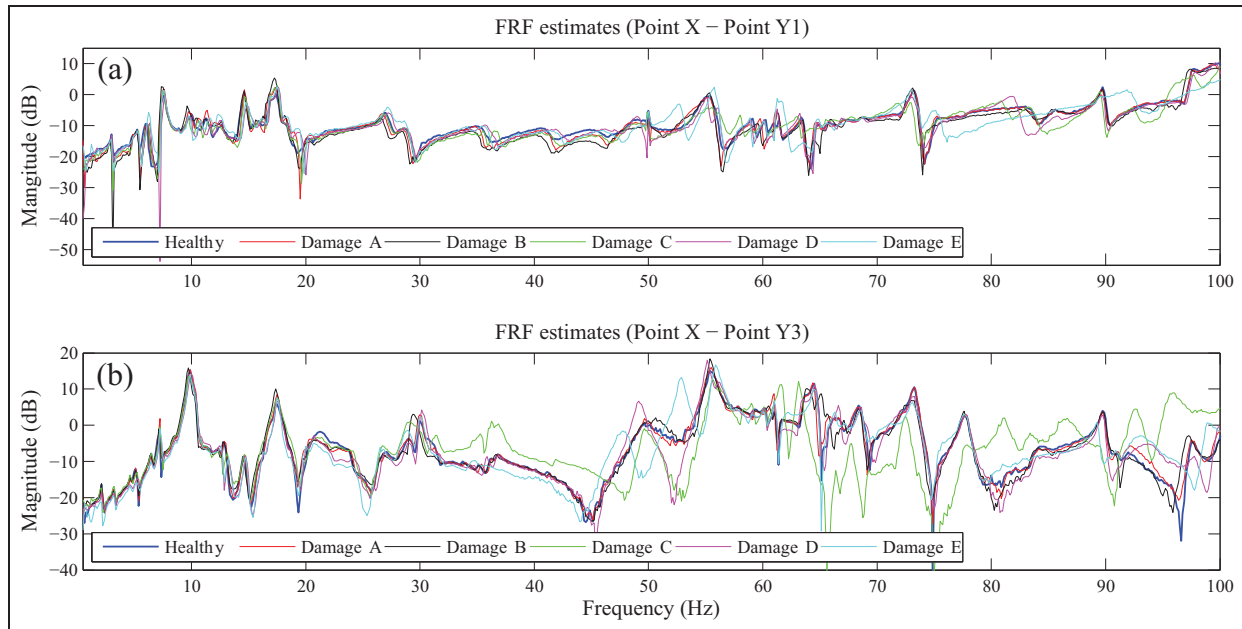


Figure 5. Frequency response function (FRF) magnitude estimates for the healthy and damage structural states: (a) Point X–Point Y1 and (b) Point X–Point Y3 transfer functions.

be observed, the healthy and damage curves are rather similar for both transfer functions in the 0.5–30 Hz range, where the first 12 modes are included. In the case of Point X–Point Y3 transfer function, significant deviations between the healthy and damage types C, D, and E curves are seen in the 30–58 Hz range, where the next three modes are included. Finally, in the 58–100 Hz range where the next eight modes are included, the Point X–Point Y1 FRF magnitude curves are quite similar except for the damage type E curve, while discrepancies are more evident for damage types C and E in the Point X–Point Y3 transfer function case.

Parametric identification. Parametric identification of the structural dynamics is based on 10,000 (≈ 39 s) sample-long excitation and single response signals that are used for estimating ARX models (MATLAB function *arx.m*). The modeling strategy consists of the successive fitting of ARX(na, nb) models (with na, nb designating the AR and X orders, respectively; in this study, $na = nb = n$) until a suitable model is selected. Model parameter estimation is achieved by minimizing a quadratic PE criterion leading to a least squares (LS) estimator.^{15,16} Model order selection is based on the BIC (Figure 6) and RSS/SSS criteria^{15,16} and the use of frequency stabilization diagrams (Figure 7).^{15,16} Stabilization diagrams depict the estimated modal parameters (usually frequencies) as a function of increasing model order n . Based upon them, model adequacy is considered attained as soon as the estimated

parameters cease to change (“stabilize”) with increasing model order.

An approximate plateau in the BIC sequences is achieved for model order $n > 100$ (Figure 6). Furthermore, as indicated in the frequency stabilization diagrams of Figure 7, model orders of $n > 90$ are adequate for most natural frequencies to get stabilized. Notice the color bars in Figure 7, which demonstrate the damping ratios for each frequency for increasing model order. In the 0.5–50 Hz range, higher damping ratios for model order $n < 100$ are observed for certain structural modes.

The above procedure leads to the selection of an ARX(112, 112), ARX(136, 136), and ARX(103, 103) model for vibration measurement positions Y1, Y2, and Y3, respectively. The selected ARX models as well as their estimation details and the corresponding numbers of the estimated parameters, samples per parameter (SPP—refers to signal samples per estimated parameter), BIC, and RSS/SSS values are summarized in Table 2. Note that the identification procedure generally leads to different ARX models (including somewhat different model orders) for each vibration measurement position.

Inspection phase

It is worth mentioning that in each test case within the inspection phase, the approach operates in an online fashion, with each signal sample being processed at a

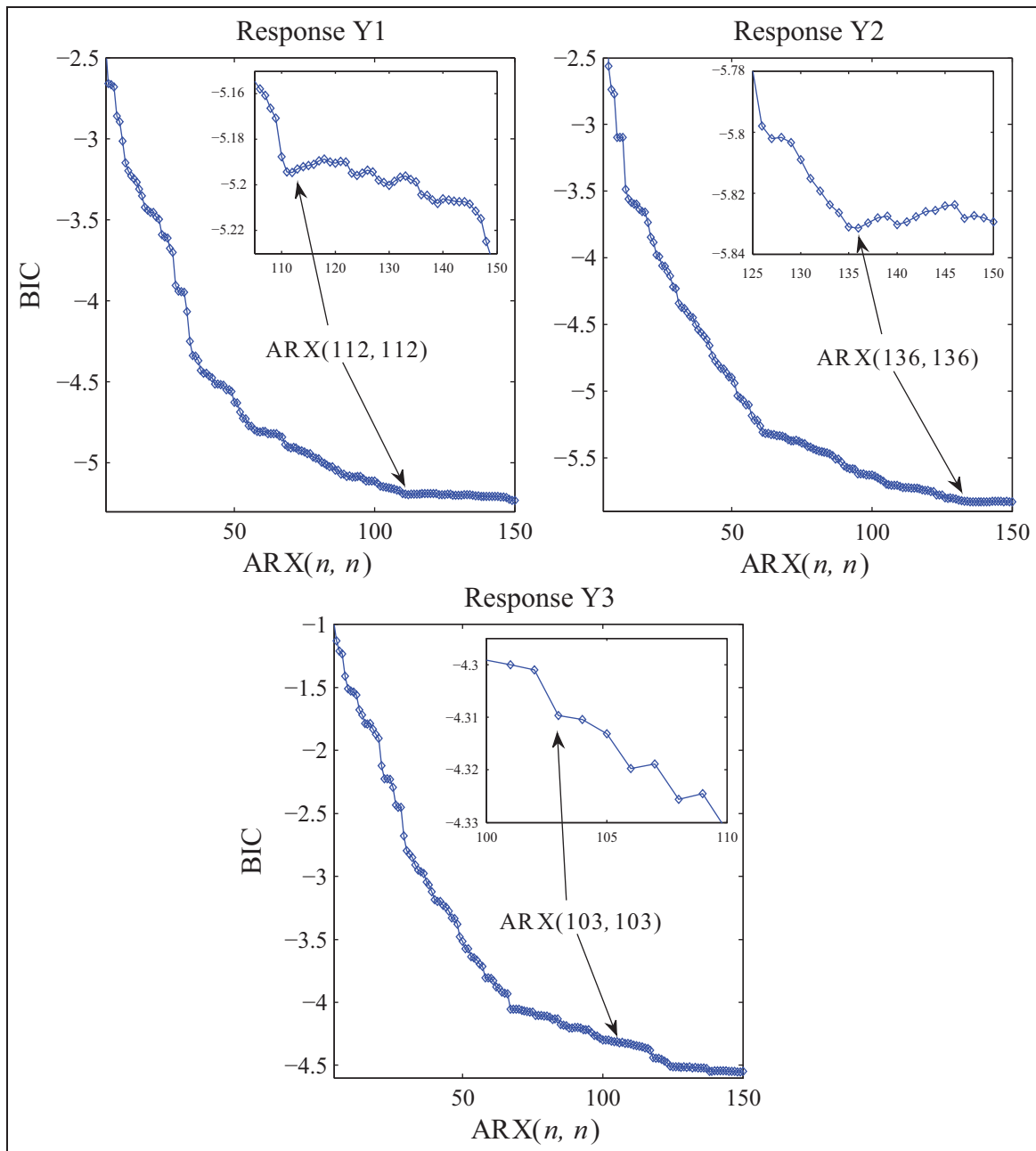


Figure 6. BIC order selection criterion for $ARX(n, n)$ type parametric models in the healthy case for all vibration response measurement positions.

time. The approach is interrupted when a test case is finished and re-started as soon as a new one is initiated.

Damage detection. Damage detection is based on the binary SPRT presented in section “Damage detection.” Prior to implementing the SPRT for tackling damage detection, an appropriate sampling plan should be selected. The selection of the sampling plan involves the determination of the following three aspects: (1) the

nominal residual standard deviation σ_o under which the structure is considered to be in its healthy state; (2) the standard deviation ratio $q = \sigma_1/\sigma_o$, which constitutes the standard deviation increase under which the structure is determined to be damaged; and (3) the SPRT strength (α, β) .

The determination of the nominal residual standard deviation σ_o under which the structure is considered to be healthy is based on the available 100 baseline experiments obtained from the healthy structure (Table 1).

Table 2. Selected models and estimation details.

Response	Selected model	No. of estimated parameters	SPP	BIC	RSS/SSS (%)
Y1	ARX(112, 112)	225 parameters	44.4	-5.19	0.43
Y2	ARX(136, 136)	273 parameters	36.6	-5.83	0.22
Y3	ARX(103, 103)	207 parameters	48.3	-4.31	1.07

Parameter estimation method: WLS, QR implementation; signal length: 10,000 samples.

SPP: samples per parameter; BIC: Bayesian information criterion; RSS/SSS: residual sum of squares/signal sum of squares; WLS: weighted least squares.

Table 3. Selected nominal residual standard deviation σ_o values for the damage detection SPRT.

	Response Y1	Response Y2	Response Y3
Nominal σ_o	0.0866	0.0660	0.1168
σ_o obtained as $E\{\hat{\sigma}\} + 1.96 \cdot \text{std}\{\hat{\sigma}\}$ out of 100 baseline residual sequences			

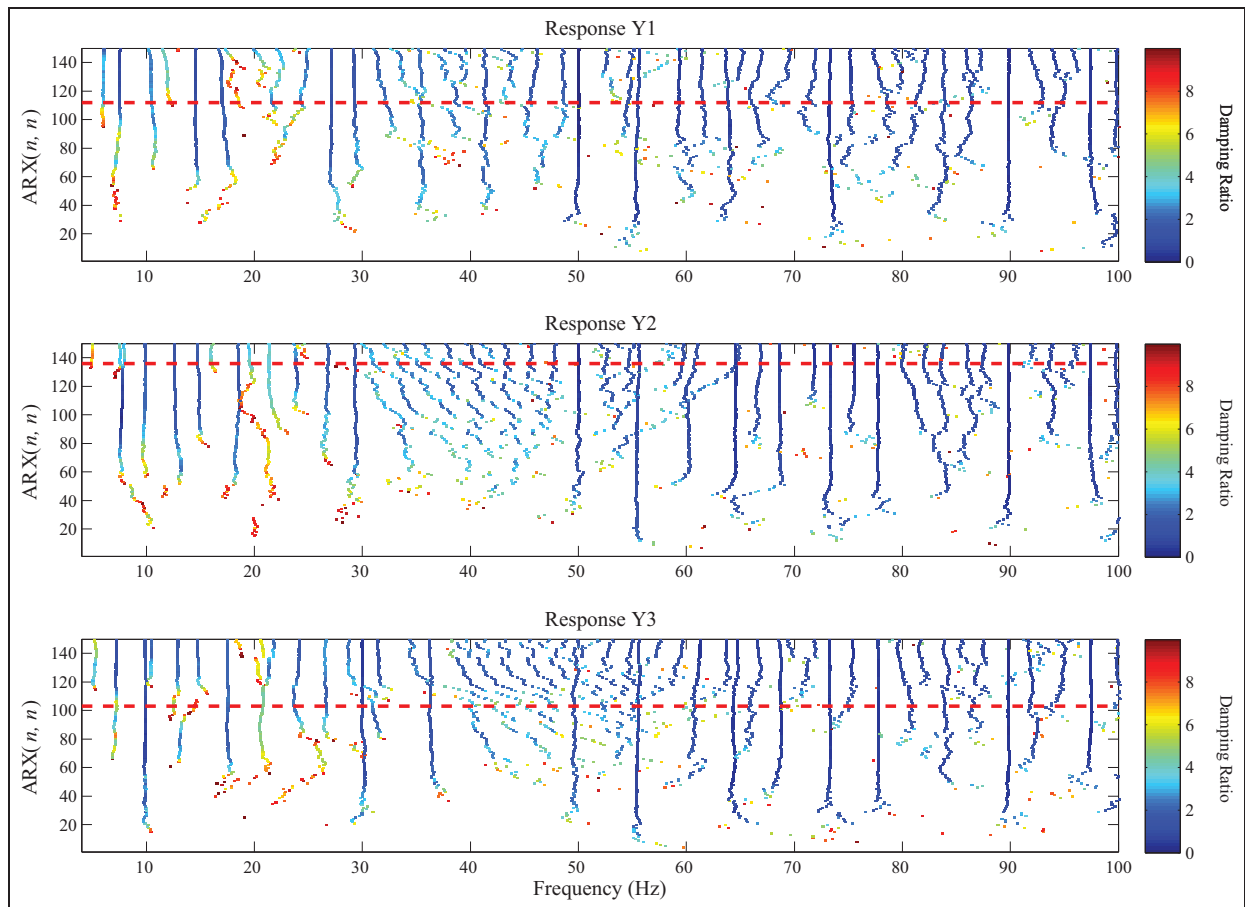


Figure 7. Frequency stabilization diagram for ARX(n, n) type models in the healthy case for all vibration response measurement positions. The dashed red lines indicate the selected model orders in each case.

For each considered vibration measurement position (Figure 4, Points Y1, Y2, and Y3), the corresponding identified ARX model, as presented in section “Parametric identification” and Table 2, is employed in

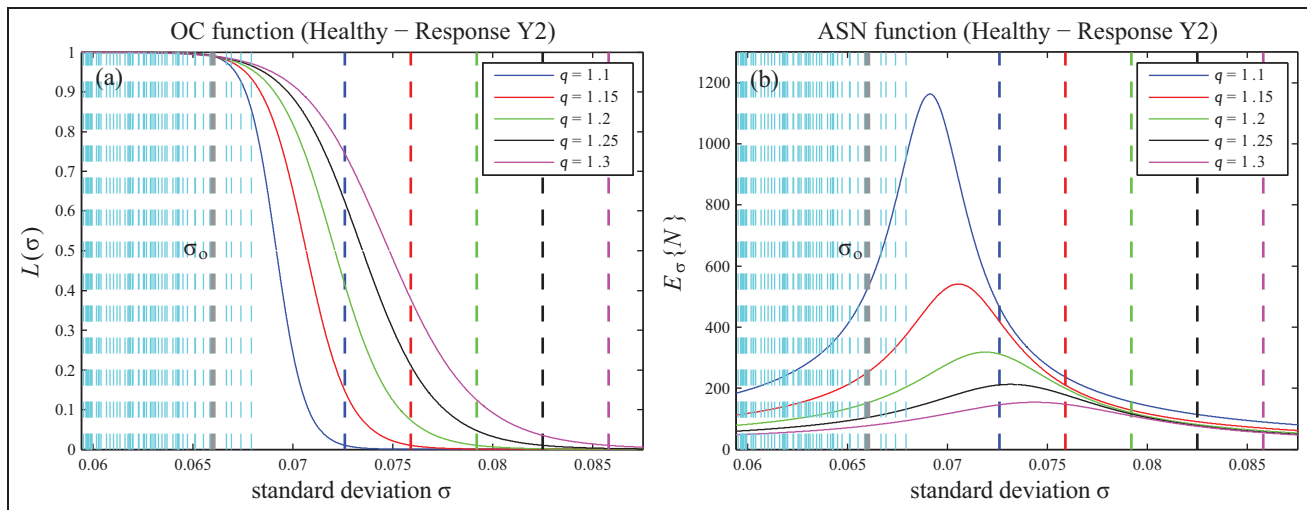


Figure 8. Healthy structure: (a) operating characteristic (OC) and (b) average sample number (ASN) functions for various residual standard deviation ratios $q = \sigma_1/\sigma_o$ and constant strength $(\alpha, \beta) = 0.01$ (vibration response Y2). The vertical colored dashed lines designate the σ_1 values for the corresponding ratios q . The vertical cyan dashed lines represent the residual standard deviation values obtained from the 100 baseline healthy experiments.

order to obtain the 100 baseline residual sequences. A typical selection for the nominal residual standard deviation value σ_o would be such that the probability of $\sigma \leq \sigma_o$ is equal to 95% ($P(\sigma \leq \sigma_o) = 0.95$). The selected nominal σ_o values for all three vibration responses are presented in Table 3.

The determination of the residual standard deviation ratio q may be based on the OC and ASN functions of the SPRT (section “Damage detection”) for various q ratios, along with the use of the baseline healthy data records. Figure 8(a) and (b) presents, for vibration response Y2, the OC and ASN functions, respectively, for various candidate ratios q and constant SPRT strength $(\alpha, \beta) = 0.01$. In both figures, the σ_o value is shown as gray vertical dashed line, while the σ_1 values corresponding to the considered $q = \sigma_1/\sigma_o$ ratios are shown in colored vertical dashed lines. Along with the OC and ASN function curves, the standard deviation values obtained from the 100 baseline residual sequences are depicted in vertical cyan dashed lines.

In Figure 8(a), the intersections of the vertical lines, belonging to the residual standard deviation values, with the OC function curves for the various q ratios correspond to the probabilities of acceptance of the null hypothesis H_o (healthy structure) for each ratio. In Figure 8(b), the intersections of the vertical lines with the ASN function correspond to the expected number of residual samples required to reach a decision. The OC function (Figure 8(a)) is considered more favorable; the higher the value of $L(\sigma)$ for σ consistent with H_o and the lower the value of $L(\sigma)$ for σ not consistent with H_o . Thus, by plotting the OC and ASN functions,

not only an indication of the probability of acceptance for various residual standard deviations σ is provided, but also an approximation to the number of residual samples required for reaching a terminal decision is given.

In order to design a robust, yet effective in detecting small damages, SPRT for damage detection, the lowest q ratio with the highest probabilities of acceptance of the null hypothesis H_o for the plotted baseline residual standard deviations should be selected. In a second stage, the expected number of residual samples required to reach a decision should be checked in order to assure that its value is in accordance with the experimental specifications and the potential online implementation requirements. Notice that the lower the selected ratio q , the greater the expected number of the required samples to reach a terminal decision. Moreover, notice that the largest amount of residual samples required to reach a decision arises when the value of the current standard deviation σ lies in the middle of the (σ_o, σ_1) range. This is due to the fact that in this case, the standard deviation σ favors neither the null H_o (healthy structure) nor the alternative H_1 (damaged structure) hypothesis. For tackling damage detection in the aluminum truss structure, a standard deviation ratio $q = \sigma_1/\sigma_o$ equal to 1.1 is selected as adequate for the implementation of the SPRT.

After the selection of the residual standard deviation ratio q , the final SPRT strength (α, β) should be determined as well. Similarly to the q selection procedure, Figure 9(a) and (b) depicts the OC and ASN functions, respectively, for various test strengths (α, β) and

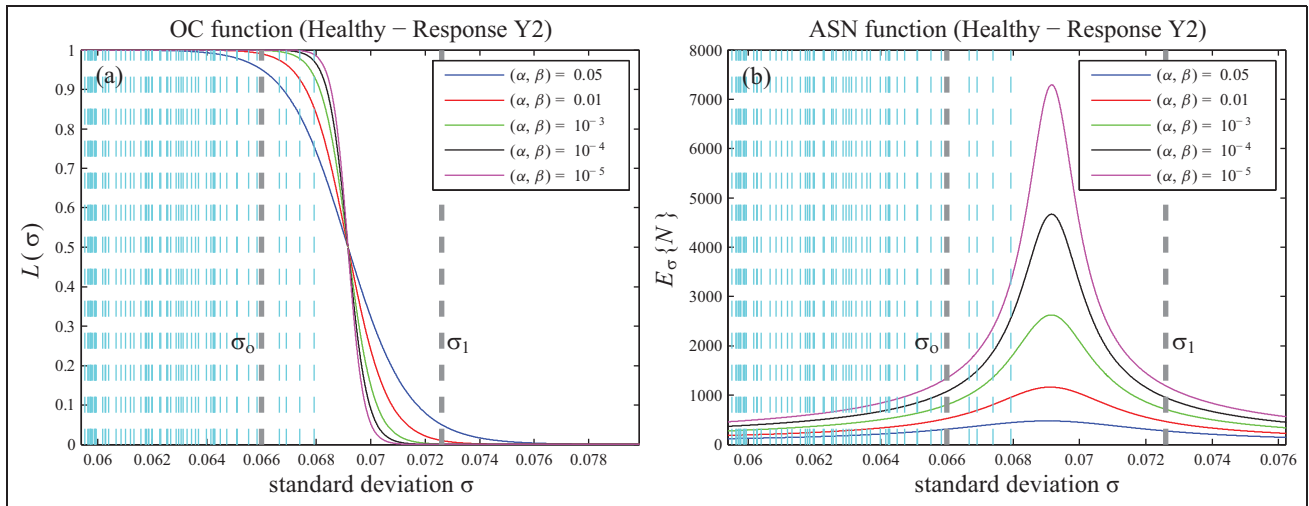


Figure 9. Healthy structure: (a) operating characteristic (OC) and (b) average sample number (ASN) functions for various strengths (α, β) and residual standard deviation ratio $q = \sigma_1/\sigma_0 = 1.1$ (vibration response Y2). The vertical cyan dashed lines represent the residual standard deviation values obtained from the 100 baseline healthy experiments.

constant ratio $q = 1.1$. Again, the standard deviation values for the baseline residual sequences are shown in vertical cyan dashed lines. Based on the standard deviation acceptance probabilities under the null hypothesis H_0 (Figure 9(a)) and the corresponding expected number of the required residual samples to reach a decision (Figure 9(b)), the user may select an appropriate strength (α, β) . Notice that the lower the selected α, β values, the greater the expected number of required samples to reach a terminal decision. For tackling damage detection in the aluminum truss structure, an SPRT strength equal to $(\alpha, \beta) = 0.01$ is selected as adequate.

Figure 10(a) and (b) depicts the OC and ASN function curves (response Y3), respectively, for various candidate ratios q and constant SPRT strength $(\alpha, \beta) = 0.01$, along with the standard deviation values (vertical cyan dashed lines) obtained from the 100 baseline residual sequences that belong to damage type A (see Table 1). In the case where baseline data from various potential damage types are available, either by corresponding experiments or tuned FE models, Figure 10(a) constitutes an additional means of validation of the determined SPRT sampling plan for damage detection. If for the selected sampling plan the probability of acceptance of damage type A standard deviation values is considerably high (vertical axis of Figure 10(a)), then there is an increased probability of missed damage occurrence, as the adopted sampling plan will not be able to clearly distinguish the standard deviation values between the healthy and the damage structural state. Furthermore, Figure 10(b) depicts the expected number

of residual samples that are required to reach a terminal decision versus the damage type A standard deviation values. As it may be observed, all the plotted baseline standard deviation values require less than 200 samples in order to accept the underlying alternative hypothesis H_1 (damaged structure).

Indicative damage detection results for vibration response Point Y1 based on the SPRT sampling plan of standard deviation ratio $q = 1.1$ and strength $(\alpha, \beta) = 0.01$ are presented in Figure 11. A damage is detected when its test statistic (vertical axis) exceeds the upper critical point (dashed horizontal lines), while the structure is determined to be in a healthy state when the test statistic exceeds the lower critical point. After a critical point is exceeded, a decision is made, while the test statistic is reset to 0 and the test continues. Hence, during testing, multiple decisions are made, as each inspection residual sequence contains 1000 samples. Evidently, correct detection (Figure 11) is obtained in each test case, as the test statistic is shown to exceed multiple times (multiple correct detections) the lower critical point in the healthy case, while it also exceeds multiple times the upper critical point (multiple correct damage detections) in the damage test cases. Inside each subplot of Figure 11 is indicated whether the corresponding damage type is “local” or “remote” with respect to the vibration sensor employed. Thus, damage types A and B are characterized as “local” with respect to sensor Y2, while damage types C, D, and E are characterized as “remote.” Observe that damage type A (Table 1) appears harder to detect, as the number of detections in this case is the smallest one among

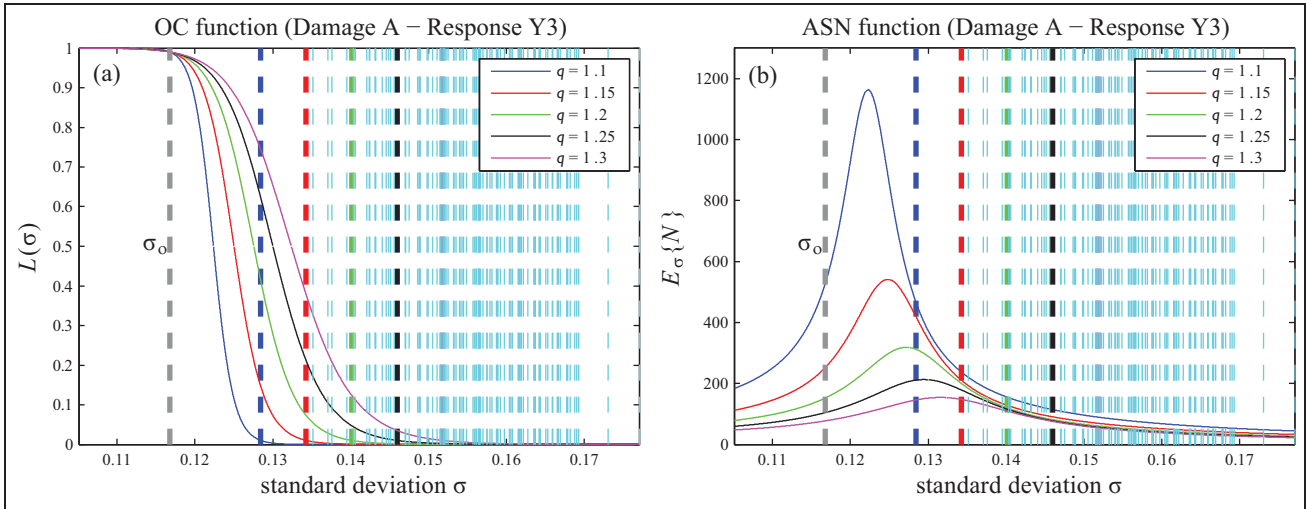


Figure 10. Damage type A: (a) operating characteristic (OC) and (b) average sample number (ASN) functions for various residual standard deviation ratios $q = \sigma_1/\sigma_o$ and constant strength $(\alpha, \beta) = 0.01$ (vibration response Y3). The vertical cyan dashed lines represent the residual standard deviation values obtained from the 100 baseline damage type A experiments.

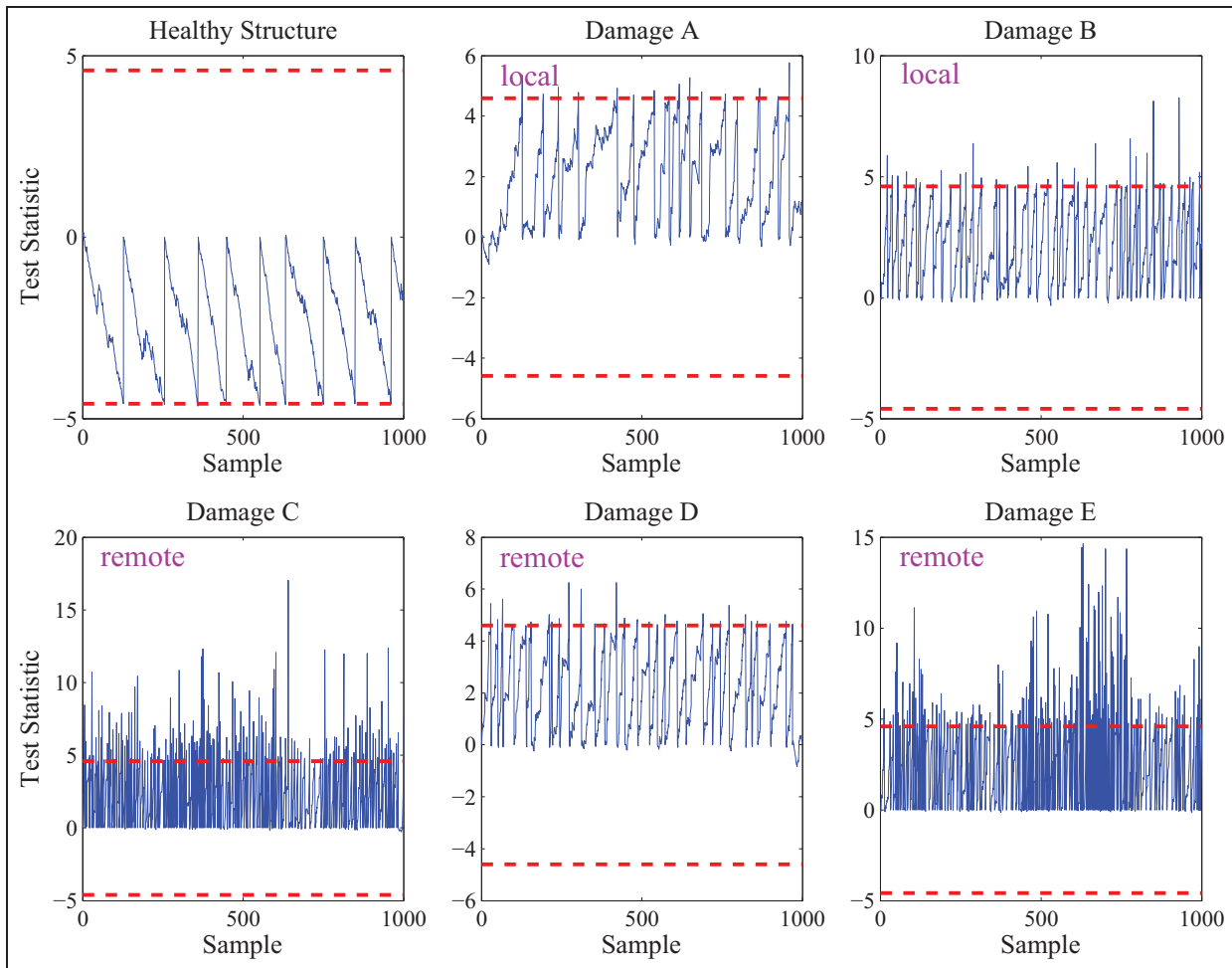


Figure 11. Indicative damage detection results for response Y2 at the $\alpha = \beta = 0.01$ risk levels ($q = \sigma_1/\sigma_o = 1.1$). The actual structural state is shown above each plot.

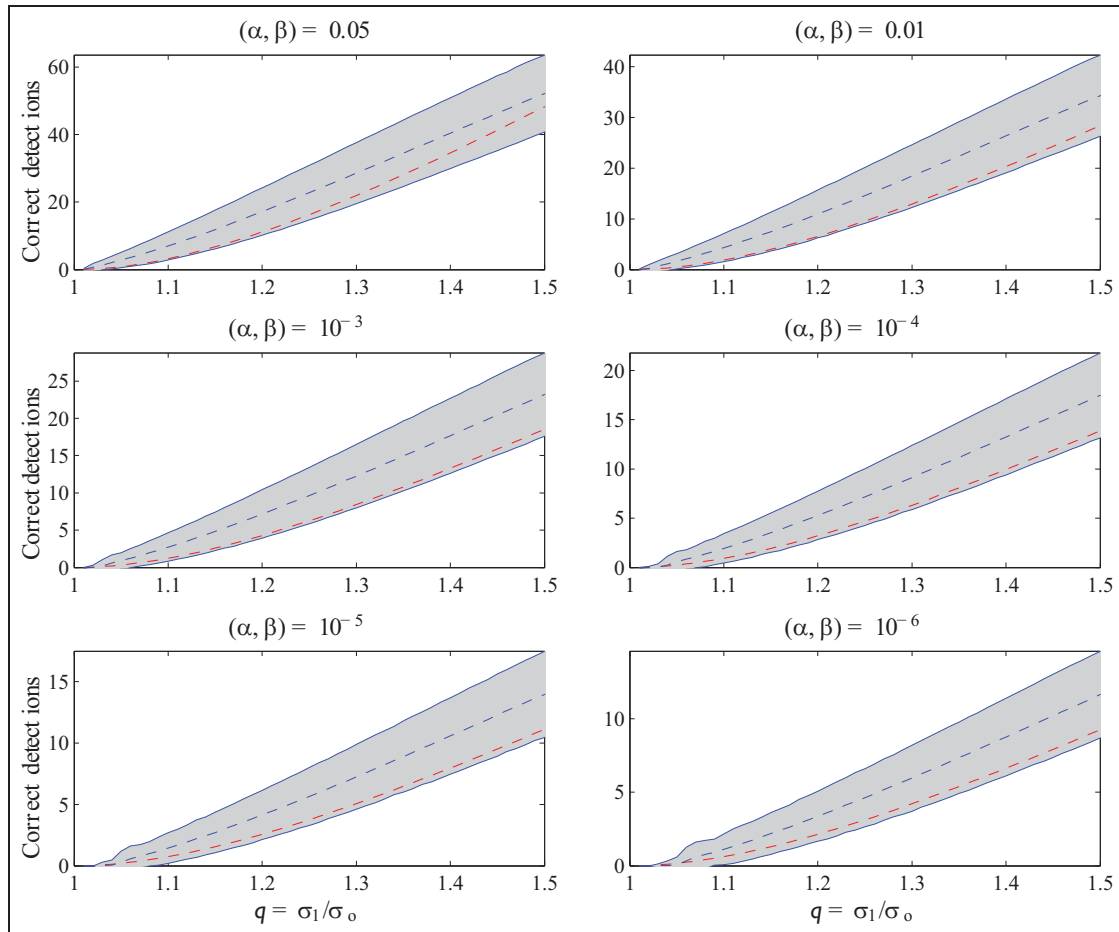


Figure 12. Average number of correct detections for the healthy structure (response Y2): experimental (dashed blue lines ± 1.96 standard deviation confidence intervals from 1100 inspection healthy experiments of 1000 samples each) and theoretical (dashed red lines) point estimates for various SPRT strengths (α, β) versus residual standard deviation ratio $q = \sigma_1/\sigma_0$. The actual strength is shown above each plot.

all the damage test cases, while damage types C and E appear easier to detect. This is in agreement with the remarks made in subsection “Non-parametric identification” and Figure 5.

Figure 12 depicts the average number of correct detections under the healthy structural state versus the residual standard deviation ratio q for various SPRT strengths (α, β) . The dashed blue lines correspond to the experimental correct detection point estimates obtained from the 1100 healthy inspection experiments of 1000 samples each, while the gray shaded areas correspond to the ± 1.96 standard deviation confidence intervals. The dashed red lines correspond to the theoretical number of correct detections as approximated via the ASN function under the null hypothesis H_0 (healthy structure). Notice that the greater the α, β error probabilities, the larger the number of correct detections per data set. Nevertheless, keep in mind that increased values of type I and II error probabilities

may lead to increased false alarm and missed damage rates.

Moreover, notice that the theoretical numbers of correct detections for the various test strengths in Figure 12 are smaller than the corresponding experimental ones in all test cases. This is due to the fact that in “real-life” applications, the experimental data often heavily favor either the null (H_0) or the alternative (H_1) hypothesis. In this case, the experimental inspection data sets were obtained under the healthy structural state, thus the corresponding residual samples strongly favor the null hypothesis of the healthy structure. This constitutes a strong indication that the proposed approach may actually perform effectively in “real-life” applications.

Figure 13 presents the false alarm percentages for all three vibration measurement locations versus the residual standard deviation ratio q for various SPRT strengths (α, β) . These rates have been extracted from the 1100 healthy inspection experiments and the

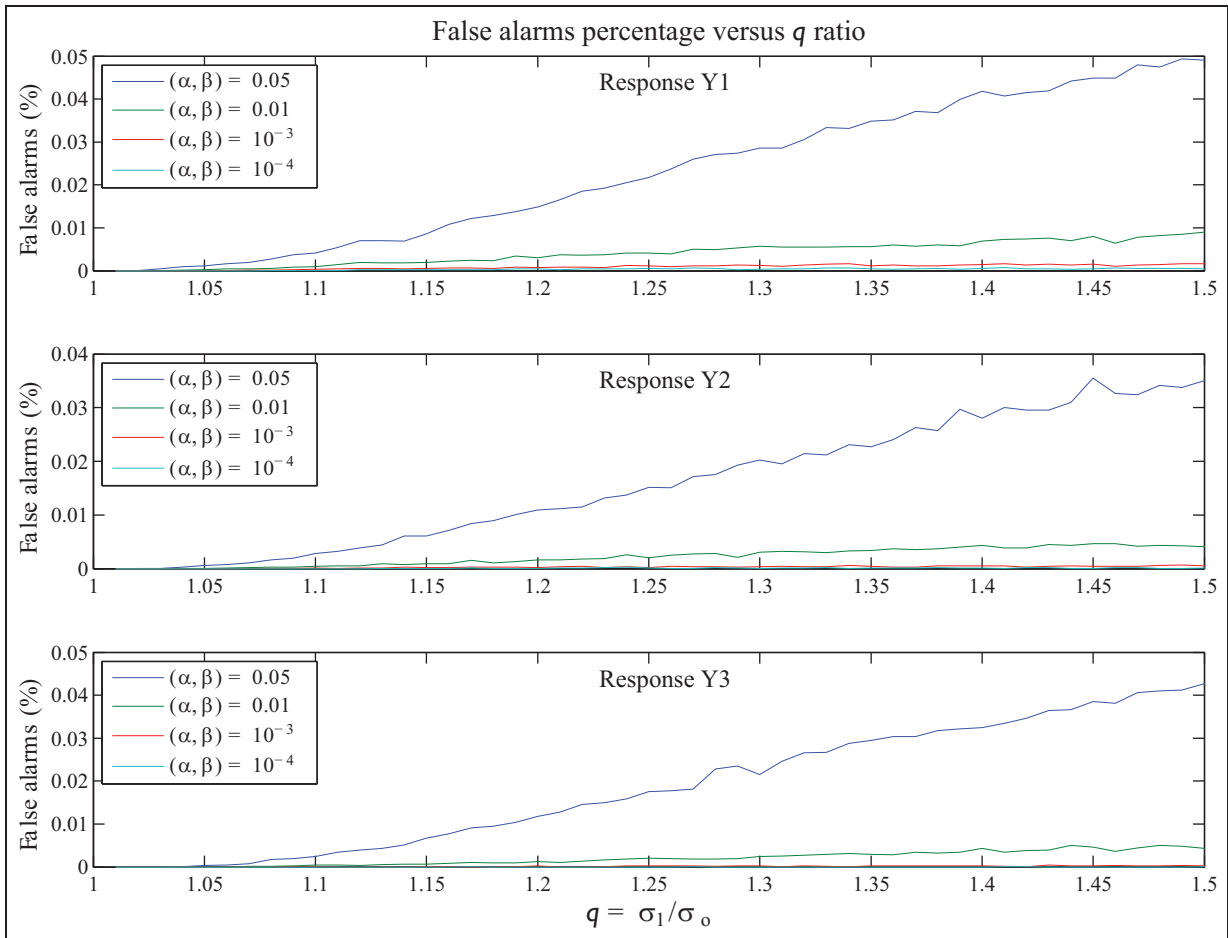


Figure 13. False alarm percentage for all vibration response measurement positions and various SPRT strengths (α, β) versus residual standard deviation ratio $q = \sigma_1/\sigma_0$; 1100 healthy inspection experiments are used.

corresponding residual sequences. As the ratio q increases, the false alarm percentages slightly increase too. This may seem awkward at first, as one would expect that as the standard deviation q increases the false alarm rates would decrease. Nevertheless, this is not the case, as by increasing the ratio q the number of correct detections largely increases (see Figure 12), and as a result, as the SPRT becomes more “sensitive,” there is a slight increase in the false alarms.

Notice that the false alarm percentages of Figure 13 are practically 0, a fact that demonstrates the effectiveness and robustness of the designed test.

Finally, Figure 14 depicts the average number of correct detections for the three vibration responses and various test strengths (α, β) under damage type A versus the residual standard deviation ratio q . The lowest mean correct detection values are obtained for vibration response Y1, while the largest values are obtained for vibration response Y3. This implies that damage type A, which is the least severe among all considered damages, is easily detected via vibration response Y3

and harder via response Y1. Nevertheless, it is obvious from Figure 14 that the SPRT is capable of accurately detecting the least severe damage type via all the considered vibration measurement locations.

The summarized damage detection results for all vibration responses are presented in Table 4. The healthy detections and false alarm numbers are mean estimates per data set, as they are extracted from the 1100 healthy inspection experiments of 1000 samples each. For all the considered vibration responses, the mean false alarm values are extremely low, as well as the mean missed damage values which are 0, except for the case of the less severe damage type A (see Figures 4 and 5 and Table 1), which exhibits its maximum mean value of false alarms for response Y1 equal to 0.39.

Overall, the approach exhibits excellent performance in tackling damage detection.

Damage identification and quantification. Damage identification and quantification are based on the multihypothesis SPRT presented in section “Damage identification

Table 4. Damage detection summary results for the three vibration responses (Y1, Y2, and Y3).

Response	Damage detection						
	Mean healthy detections	Mean false alarms	Mean missed damage values				
			Damage A	Damage B	Damage C	Damage D	Damage E
Y1	4.40	0.011	0.390	0	0	0	0
Y2	4.34	0.005	0.048	0	0	0	0
Y3	3.61	0.005	0	0	0	0	0

Test strength $(\alpha, \beta) = 0.01$; residual standard deviation ratio $q = \sigma_1/\sigma_0 = 1.1$.
 Mean healthy detections and false alarms per data set out of 1100 healthy inspection experiments.
 Mean missed damage values per data set out of 900 damage inspection experiments.

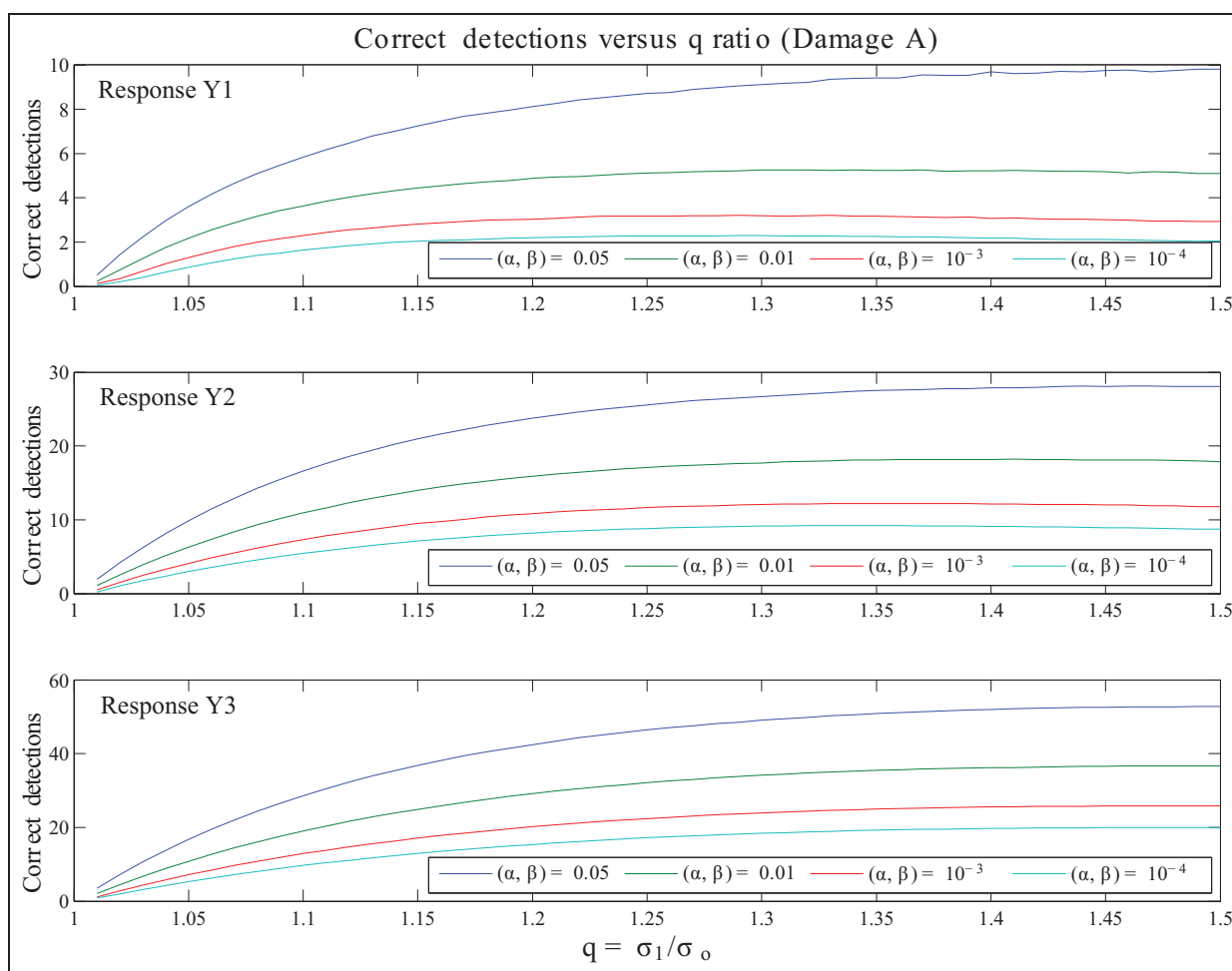


Figure 14. Average number of correct damage detections under damage type A for all vibration response measurement locations and various SPRT strengths (α, β) versus residual standard deviation ratio $q = \sigma_1/\sigma_0$; 800 damage type A inspection experiments are used.

and quantification.” Prior to implementing the multihypothesis test for tackling damage identification and quantification, an appropriate sampling plan should be selected, similarly to the damage detection task. The selection of the sampling plan involves the

determination of the following two aspects: (1) the nominal residual standard deviation values $\sigma_A, \dots, \sigma_E$ under which the structure is considered to be in the corresponding damage types A, ..., E state, respectively, and (2) the matrix of error probabilities α_{ij} and the

Table 5. Nominal residual standard deviation values $\sigma_A, \dots, \sigma_E$ for damage identification.

Response	Nominal residual standard deviations				
	σ_A	σ_B	σ_C	σ_D	σ_E
Y1	0.1056	0.1617	0.2304	0.1492	0.3259
Y2	0.0991	0.1361	0.2672	0.1211	0.2806
Y3	0.1633	0.3377	1.7264	0.3475	0.4857

$\sigma_A, \dots, \sigma_E$ mean values out of 100 baseline damage data sets each.

vector of correct decision probabilities α_{ii} (see equation (19)).

The determination of the nominal residual standard deviation values $\sigma_A, \dots, \sigma_E$ under which the structure is considered to be under the corresponding damage type is based on the available 100 baseline experiments obtained from the structure under each damage state (Table 1). For each considered vibration measurement position (Figure 4; Points Y1, Y2, and Y3), the corresponding identified ARX model, as presented in section "Parametric identification" and Table 2, is employed in order to obtain the 100 baseline residual sequences for each damage type. In the damage identification and quantification case, the nominal residual standard deviation values $\sigma_A, \dots, \sigma_E$ that are needed to implement the multihypothesis test are selected as the mean values of the 100 baseline residual standard deviations under each damage type. The selected nominal $\sigma_A, \dots, \sigma_E$ values for all three vibration responses are presented in Table 5.

As it may be observed from Table 5, the nominal residual standard deviation values σ_B and σ_D , that belong to damage types B and D, respectively, are quite similar for all three vibration response positions. This is due to the fact that these two damage types have a similar effect on the residual sequences obtained by driving the baseline data under each damage type through the nominal models of the healthy structure (see Table 2).

Indicative damage identification results for vibration response Y1 at the $\alpha_{ij} = 0.01$ error probabilities level are presented in Figure 15, with the actual damage being of type C. Inside each subplot of Figure 15 is indicated whether the considered damage type is "local" or "remote" with respect to the vibration sensor employed (sensor Y1), hence damage type C is characterized as "local," whereas damage types A, B, D, and E are characterized as "remote." The vertical axis in each subplot designates whether the corresponding hypothesis is accepted or rejected, while the horizontal axes indicate the residual samples. Once the multihypothesis test reaches a terminal decision the corresponding damage type hypothesis is accepted; thus, the sample for which this terminal decision is made constitutes the stopping time of the test (see equations (17)

and (18)). In Figure 15, the hypotheses belonging to damage types A, B, D, and E are correctly rejected, while the hypothesis that belongs to damage type C is correctly accepted. Moreover, notice that the stopping time for the terminal decision of hypothesis C acceptance is reached before 50 samples (≈ 0.19 s), which demonstrates the ability of the multihypothesis test to arrive at an early decision.

Summary identification results for all vibration responses are presented in Table 6. The correct damage classification rates are presented for all damage type inspection sets, along with the corresponding mean stopping times. As it may be observed, the multihypothesis test's damage classification results obtained for all vibration responses are very accurate for damage types A, C, and E, as the percentages of correct classification are very high. Nevertheless, the approach faces difficulties in accurately classifying damage types B and D. As already mentioned, this is due to the fact that these damage types have a similar effect on their corresponding residual standard deviation values obtained through the healthy models (see Tables 2 and 5).

In this case, the user may apply the binary SPRT for the candidate damage types. Nevertheless, this procedure would require the baseline modeling of at least one of these types.

Indicative damage identification results for damage types B and D via the binary SPRT at the $\alpha = \beta = 0.01$ risk levels and $q = \sigma_1/\sigma_o = 1.1$ are presented in Figure 16 for vibration response Y2. The model orders that were employed for the ARX modeling of damage types B and D are the same that are used for the modeling of the healthy structure (Table 2). As it may be observed from Figure 16, although the multihypothesis approach faces difficulties in correctly classifying these damage types, the binary SPRT is capable of accurately identifying the actual damage type as current, while the summarized results exhibit zero misclassification numbers. Nevertheless, this approach requires the baseline modeling of the potential damage structural states, a procedure that is avoided by the multihypothesis approach.

Damage quantification is indirectly treated via the damage identification task. The nominal residual

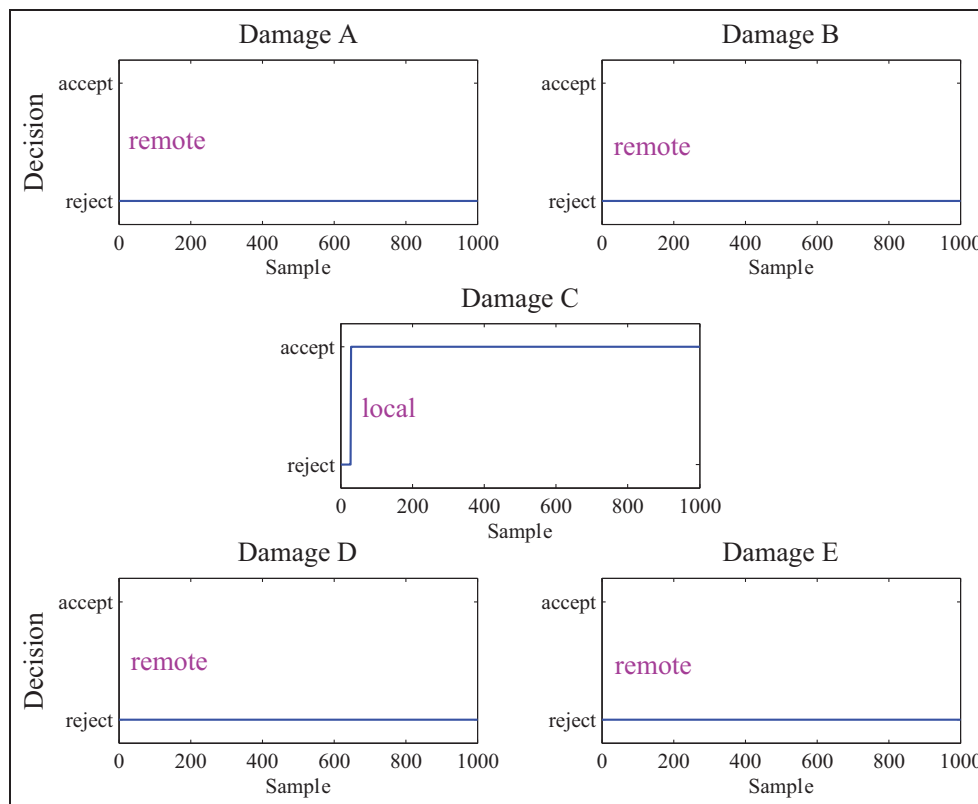


Figure 15. Indicative damage identification results for response Y1 at the $\alpha_{ij} = 0.01$ error probabilities' level, with the actual damage being of type C. The hypothesized structural state is shown above each plot.

Table 6. Damage identification summary results for the three vibration responses (Y1, Y2, and Y3).

Actual damage	Damage identification (correct damage classification rates (%))				
	Damage A hypothesis	Damage B hypothesis	Damage C hypothesis	Damage D hypothesis	Damage E hypothesis
Type A	99.33/98.22/100	0.11/0/0	0/0/0	0.55/1.78/0	0/0/0
Type B	0/0/0	45.65/69.77/66.55	2.33/0/0	52/30.22/33.44	0/0/0
Type C	0/0/0	0/0/0	98.32/95.10/100	0/0/0	0.66/4.89/0
Type D	0/0/0	46.33/11.22/49.99	0/0/0	53.55/88.77/51.01	0/0/0
Type E	0/0/0	0/0/0	0.11/1.11/0.77	0/0/0	99.88/98.88/97.65
Mean stop. time	15.68/22.84/8.76	174.35/172.32/176.26	36.18/117.99/3.81	200.08/167.34/231.98	18.54/90.33/27.21

Correct damage classification rate for points Y1/Y2/Y3 out of 800 inspection experiments; $\alpha_{ij} = 0.01$.

Mean stopping time in samples for points Y1/Y2/Y3 out of 800 inspection experiments each providing 1000-sample long signals.

Bold values indicate the results in which the damage hypothesis corresponds to the actual damage type.

standard deviation values $\sigma_A, \dots, \sigma_E$, as determined in the multihypothesis damage identification approach, constitute an indication of damage severity for the corresponding damage types. This is due to the fact that as damage severity increases, the current structural dynamics deviate from the nominal healthy behavior, thus the nominal model belonging to the healthy structure will not be able to accurately represent them, leading to increased residual sequence values and corresponding standard deviations.

Table 5 presents the selected nominal standard deviation values for all damage types (see also Figure 4). For vibration responses of Points Y1 and Y2, damage type E is the most severe followed by damage type C. Damage types B and D are of the same severity level, which justifies the misclassification issues for these types, while damage type A is the least severe and thus hardest to detect. For the vibration response of Point Y3, damage type C is the most severe, followed by damage type E. Again, damage types B and D are

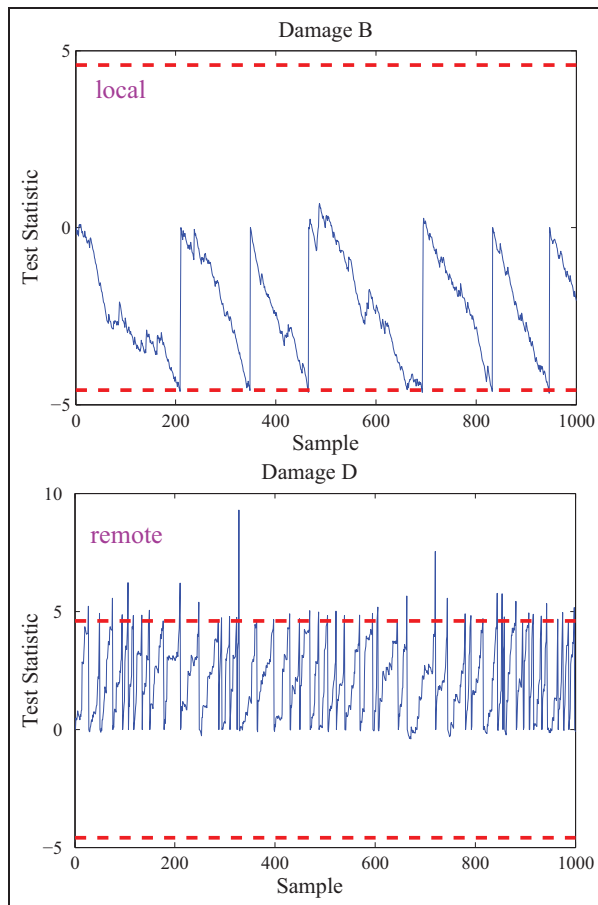


Figure 16. Indicative damage identification results for response Y2 at the $\alpha = \beta = 0.01$ risk levels ($q = \sigma_1/\sigma_0 = 1.1$) for damage types B and D. The baseline model of damage type B is used with the actual structural state shown above each plot.

of the same severity level, while damage type A is the least severe. The above conclusions are in agreement with the parametric FRF curves presented in Figure 5 and the remarks of subsection “Non-parametric identification.”

Concluding remarks

An SPRT framework for vibration-based SHM was postulated. This framework, which is based on binary and multihypothesis versions of the statistically optimal SPRT, was shown to be capable of achieving effective and early damage detection and identification. The main conclusions drawn may be summarized as follows:

- The proposed framework was shown to effectively tackle damage detection and identification, achieving excellent performance with practically zero false alarms and missed damage rates.

- An optimal sampling plan was determined a priori via the use of the OC and ASN functions, selected type I (false alarm) and II (missed damage) error probabilities, and available baseline data records of the structure under various potential health states.
- The framework was shown to achieve *early* damage detection and identification (<0.19 s) as it required a minimum number of residual samples in order to reach a decision. In addition, it was shown to have global and robust damage detection capabilities, as it was able to detect damage using sensors that were either “local” or “remote” to the damage location.
- The multihypothesis damage identification procedure faced some difficulties in classifying two damage types with similar effects on the residual series. Yet, this issue was effectively tackled via the baseline modeling of these damage types and sequential binary hypothesis testing.
- The availability of baseline data records corresponding to various potential damage scenarios is necessary in order to treat damage identification. This may not always be possible with the actual structure itself, but laboratory scale models or analytical (FE) models may be used for this purpose.
- The approach uses simple time series models (ARX, ARMAX, state space, etc.) and is characterized by computational simplicity; features that enhance its attractiveness for online application.

Funding

This research received no specific grant from any funding agency in the public, commercial, or not-for-profit sectors.

References

1. Doebling SW, Farrar CR, Prime MB, et al. *Damage identification and health monitoring of structural and mechanical systems from changes in their vibration characteristics: a literature review*. Technical report LA-13070-MS, May 1996. Los Alamos, NM: Los Alamos National Laboratory.
2. Doebling SW, Farrar CR and Prime MB. A summary review of vibration-based damage identification methods. *Shock Vib Digest* 1998; 30(2): 91–105.
3. Farrar CR, Doebling SW and Nix DA. Vibration-based structural damage identification. *Philos T Roy Soc A* 2001; 359: 131–149.
4. Montalvão D, Maia NMM and Ribeiro AMR. A summary review of vibration-based damage identification methods. *Shock Vib Digest* 2006; 38(4): 295–324.
5. Fassois SD and Sakellariou JS. Time series methods for fault detection and identification in vibrating structures. *Philos T Roy Soc A* 2007; 365: 411–448.
6. Fassois SD and Sakellariou JS. Statistical time series methods for structural health monitoring. In: Boller C, Chang FK and Fujino Y (eds) *Encyclopedia of structural*

- health monitoring. West Sussex: John Wiley & Sons Ltd, 2009, pp. 443–472.
7. Fan W and Qiao P. Vibration-based damage identification methods: a review and comparative study. *Struct Health Monit* 2011; 10(1): 83–111.
 8. Sakellariou JS and Fassois SD. Vibration based fault detection and identification in an aircraft skeleton structure via a stochastic functional model based method. *Mech Syst Signal Pr* 2008; 22: 557–573.
 9. Kopsaftopoulos FP and Fassois SD. Vibration based health monitoring for a lightweight truss structure: experimental assessment of several statistical time series methods. *Mech Syst Signal Pr* 2010; 24: 1977–1997.
 10. Kopsaftopoulos FP and Fassois SD. A functional model based statistical time series method for vibration based damage detection, localization, and magnitude estimation. *Mech Syst Signal Pr* 2013; 39: 143–161.
 11. Sakellariou JS, Petsounis KA and Fassois SD. Vibration analysis based on-board fault detection in railway vehicle suspensions: a feasibility study. In: *Proceedings of first national conference on recent advances in mechanical engineering*, Patras, Greece, 17–20 September, 2001.
 12. Liberatore S and Carman GP. Power spectral density analysis for damage identification and location. *J Sound Vib* 2004; 274(3–5): 761–776.
 13. Bayissa WL and Haritos N. Damage identification in plate-like structures using bending moment response power spectral density. *Struct Health Monit* 2007; 6(1): 5–20.
 14. Rizos DD, Fassois SD, Marioli-Riga ZP, et al. Vibration-based skin damage statistical detection and restoration assessment in a stiffened aircraft panel. *Mech Syst Signal Pr* 2008; 22: 315–337.
 15. Ljung L. *System identification: theory for the user*. 2nd ed. Upper Saddle River, NJ: Prentice Hall, 1999.
 16. Fassois SD. Parametric identification of vibrating structures. In: Braun S, Ewins D and Rao S (eds) *Encyclopedia of vibration*. San Diego, CA: Academic Press, 2001, pp. 673–685.
 17. Sohn H and Farrar CR. Damage diagnosis using time series analysis of vibration signals. *Smart Mat St* 2001; 10: 446–451.
 18. Sohn H, Allen DW, Worden K, et al. Statistical damage classification using sequential probability ratio tests. *Struct Health Monit* 2003; 2(1): 57–74.
 19. Nair KK, Kiremidjian AS and Law KH. Time series-based damage detection and localization algorithm with application to the ASCE benchmark structure. *J Sound Vib* 2006; 291: 349–368.
 20. Zheng H and Mita A. Two-stage damage diagnosis based on the distance between ARMA models and pre-whitening filters. *Smart Mat St* 2007; 16: 1829–1836.
 21. Carden EP and Brownjohn JM. ARMA modelled time-series classification for structural health monitoring of civil infrastructure. *Mech Syst Signal Pr* 2008; 22(2): 295–314.
 22. Gao F and Lu Y. An acceleration residual generation approach for structural damage identification. *J Sound Vib* 2009; 319: 163–181.
 23. Kopsaftopoulos FP and Fassois SD. Scalar and vector time series methods for vibration based damage diagnosis in a scale aircraft skeleton structure. *J Theor Appl Mech* 2011; 49(3): 727–756.
 24. Wald A. *Sequential analysis*. New York: Wiley, 1947.
 25. Ghosh BK and Sen PK (eds). *Handbook of sequential analysis*. New York: Marcel Dekker, Inc., 1991.
 26. Lehmann EL and Romano JP. *Testing statistical hypotheses*. 3rd ed. New York: Springer, 2008.
 27. Wald A and Wolfowitz J. Optimum character of the sequential probability ratio test. *Ann Math Stat* 1948; 19: 326–339.
 28. Humenik KE and Gross KC. Sequential probability ratio tests for reactor signal validation and sensor surveillance applications. *Nucl Sci Eng* 1990; 150: 383–390.
 29. Gross KC and Humenik KE. Sequential probability ratio tests for nuclear plant component surveillance. *Nucl Technol* 1991; 93: 131–137.
 30. Schoonewelle H, van der Hagen THJJ and Hoogenboom JE. Theoretical and numerical investigation into the SPRT method for anomaly detection. *Ann Nucl Energy* 1995; 22(11): 731–742.
 31. Schoonewelle H, van der Hagen THJJ and Hoogenboom JE. A comparison of three time-domain anomaly detection methods. *Ann Nucl Energy* 1996; 23(2): 159–170.
 32. Glöckler O. Fault detection via sequential probability ratio test of multivariate autoregressive modeling-based residual time series. In: *Sixth symposium on nuclear reactor surveillance and diagnostics*, Gatlinburg, TN, 19–24 May 1991.
 33. Oh CK and Sohn H. Damage diagnosis under environmental and operational variations using unsupervised support vector machine. *J Sound Vib* 2009; 328: 224–239.
 34. Tartakovsky AG, Li XR and Yaralov G. Sequential detection of targets in multichannel systems. *IEEE T Inform Theory* 2003; 49(4): 425–445.
 35. Emlsee B, Rogers SK, DeSimio MP, et al. Complete automatic target recognition system for tactical forward-looking infrared images. *Opt Eng* 1997; 36: 2593–2603.
 36. Veeravalli VV and Baum CW. Hybrid acquisition of direct sequence CDMA signals. *Int J Wireless Inform Network* 1996; 3: 55–65.
 37. Box GEP, Jenkins GM and Reinsel GC. *Time series analysis: forecasting and control*. 3rd ed. Englewood Cliffs, NJ: Prentice Hall.
 38. Mukhopadhyay N and De Silva BM. *Sequential methods and their applications*. Boca Raton, FL: Chapman and Hall/CRC, 2009.
 39. Tantaratana S and Thomas JB. Truncated sequential probability ratio test. *Inform Sciences* 1977; 12: 283–300.
 40. Armitage P. Sequential analysis with more than two alternative hypotheses and its relation to discriminant function analysis. *J Roy Stat Soc B Met* 1950; 12(1): 137–144.